Expansion microscopy of axonemal dyneins in islet primary cilia

Xinhang Dong[1, 2], Jung Hoon Cho[2], Jing Hughes[2*]

[1]Department of Biomedical Engineering, McKelvey School of Engineering, Washington University, One Brookings Drive, Saint Louis, MO

[2]Department of Medicine, Division of Endocrinology, Metabolism, and Lipid Research, Washington University School of Medicine, 660 South Euclid Ave, Saint Louis, MO

[*]Correspondence: jing.hughes@wustl.edu

ABSTRACT

Primary cilia are sensory organelles that mediate critical cellular functions yet are difficult to visualize because of their small size and low abundance. Expansion microscopy (ExM) is an imaging method that physically expands biological specimens using a swellable hydrogel, facilitating downstream imaging of small cellular structures. In this study, we apply ExM with confocal imaging to probe axonemal dynein expression in murine and human pancreatic islets. Innovations include an updated ExM workflow adapted from 2D cultured cells to 3D tissue optimized for intact pancreatic islets, and demonstration of axonemal dynein protein expression in islet primary cilia and centrioles. Four dynein subunits were consistently detected in both expanded and nonexpanded samples across species, including DNAI1, DNAH5, DNAH11, and DNALI1, where DNAI1 expression was the most readily detectable and seen to exhibit a distinct ring-like symmetry on super-resolution imaging. We discuss technical issues contributing to ExM success, including antibody performance across ExM and conventional sample preparation and imaging protocols, and the need to validate findings using gene knockdowns and controls. We conclude that ExM is a useful approach for identifying ciliary proteins in pancreatic islet tissue and may be broadly applicable to studying protein composition of other organelles.

Keywords Expansion microscopy, islet, primary cilia, dynein

INTRODUCTION

Cellular organelles are nanomachines with intricate molecular organization that often elude study by conventional light microscopy(Klena and Pigino 2022). Obtaining detailed structural information at the single organelle level typically requires super-resolution fluorescence microscopy or electron microscopy(Yoon et al. 2019), which can be technically challenging or inaccessible imaging modalities. Expansion microscopy (ExM) is an increasingly popular approach using a chemical strategy to expand samples to bypass the diffraction limit posed by optical physics. By embedding a specimen in a swellable hydrogel polymer and expanding it volumetrically and isotropically, ExM enables nanoscale imaging of biological samples using conventional confocal microscopes, allowing the study of cellular structures in molecular detail.

Primary cilia are hair-like projections that function as sensory and signaling organelles on eukaryotic cells. In the endocrine pancreas, islet beta and alpha cells each express a single primary cilium, whose protein composition and structure we and others have begun to explore by light and electron microscopy(Hughes et al. 2020; Cho et al. 2022; Polino et al. 2023; Müller et al. 2023). Measuring only microns in length and sub-micron in diameter, the diminutive size and solitary nature of primary cilia makes them challenging to study by imaging, especially in densely packed tissues where ciliary projections are not always clearly resolvable over the cell bodies, and antibody performance can vary in labeling efficiency and specificity. The inability to resolve individual protein localizations within islet primary cilia has been a barrier in our study of islet cilia composition, structure, and function.

We are particularly interested in axonemal dynein expression on islet primary cilia, as we had previously demonstrated using genetic and functional imaging approaches that islet beta cell cilia possess active, motor-driven movement(Cho et al. 2022; Li et al. 2022). Axonemal dynein is distinct from cytoplasmic dynein, the former considered a specialty of cells possessing motile cilia, while the latter is found in all cells and participates in fundamental cell body processes such as cargo transport and mitotic regulation(Viswanadha, Sale, and Porter 2017; Reck-Peterson et al. 2018). Axonemal dynein is a multi-subunit protein complex composed of two heavy chains containing motor and microtubule-binding domains, along with accessory light chains that provide structural integrity and support interactions with other proteins. Among these subunits, dynein axonemal intermediate chain 1 (DNAI1) is a critical component of the outer dynein arm (ODA), where mutations in the protein result in ciliary dysmotility (Zariwala et al. 2006; Ziętkiewicz et al. 2010). We had previously used immunofluorescence (IF) and immuno-scanning electron microscopy (immuno-SEM) to demonstrate DNAI1 protein expression in human and mouse islet primary cilia, along with dynein axonemal heavy chain 5 (DNAH5) (Cho et al. 2022; Sviben et al. 2024). These studies were limited however in a) the ability to resolve sub-ciliary expression patterns of dynein by conventional IF and b) the labor- and cost-intensiveness of immuno-SEM. To facilitate the detection and mapping of ciliary proteins in intact primary islets using light microscopy, we adopt ExM as a high-resolution imaging modality to systematically examine dynein protein expression on the primary cilia of mouse and human islet tissue.

METERIALS AND METHODS

Antibodies

To ensure rigor and reproducibility, we exclusively used commercially available primary and secondary antibodies for this study, with sources and staining conditions detailed in **Table 1**. Antibodies were selected on the basis of 1) published literature review, 2) vendor validation by affinity purification and knockout (KO)/knockdown (KD), and 3) performance screening in our laboratory.

MIN6 cell line

MIN6 cells were a gift from the Piston Lab at Washington University. The MIN6 cell line is a standard murine insulinoma beta cell line (Hohmeier and Newgard 2004; Nakashima et al. 2009). We used low-passage MIN6 cells between P48 to P55 to ensure healthy cell morphology and functionality (Cheng et al. 2012),. Cells were cultured in MIN6 media (DMEM supplemented with 25 mM glucose, 15% fetal bovine serum (FBS), 1% (v/v) penicillin/streptomycin, 4 mM glutamine) and passaged or used before they reach ~70% confluence.

Animals

Wild-type (WT) mice on the C57BL/6 background were used as source of mouse islets for this study. We saw no sex differences in islet cilia morphology, number, and distribution, and male-female data were pooled for quantitation. Animals were maintained in accordance with Institutional Animal Care and Use Committee regulations at the Washington University School of Medicine.

Isolation of mouse islets

Mouse islets were isolated from healthy young adult mice by pancreatectomy followed by collagenase digestion using modified Lacy protocol (Lacy and Kostianovsky 1967; Li et al. 2009). Isolated islets were recovered overnight in islet media prior to use (RPMI-1640 supplemented with 11 mM glucose, 10% FBS, 1% (v/v) penicillin/streptomycin, and 20 mM 4-(2-hydroxyethyl)-1-piperazine ethane sulfonic acid (HEPES) (Stendahl, Kaufman, and Stupp 2009; Phelps et al. 2017). Low-retention plastic and glass surfaces including tissue culture dishes and pipette tips were used to prevent islet sticking and sample loss.

Human islets

Human donor islets were sourced from the Integrated Islet Distribution Program (IIDP) and Prodo Laboratories Inc. Islets were visually inspected for morphology upon arrival and recovered overnight in islet media prior to use (RPMI-1640 supplemented with 10%

FBS, 11 mM glucose, 1% (v/v) penicillin/streptomycin, 20 mM HEPES). Both male and female islets were included in the study. Human islet use was in adherence with institutional review board (IRB) guidelines.

Sample preparation for ExM

For 2D monolayer cells: MIN6 cells were seeded and grown to approximately 70% confluence on 12 mm glass coverslips coated with poly-D-lysine (100 µg/mL) to promote cell attachment. Cells were fixed with 4% paraformaldehyde (PFA) in phosphate buffered saline (PBS) for 15 minutes at room temperature, permeabilized in 0.3% Triton X-100 in PBS for 10 minutes, washed in PBS, then incubated with freshly prepared acrylamide/formaldehyde (AA/FA) mix (final concentration 0.7% formaldehyde, 1% acrylamide in PBS) for 5-8 hours at 37°C. The freshness of this AA/FA solution was essential.

For 3D islet tissue: Intact murine and human islets were rinsed in PBS and fixed in 4% PFA for 30 minutes, permeabilized in 0.3% Triton X-100 in PBS for 10 minutes at room temperature, then treated with AA/FA mix overnight at 37°C post-fixation. A total of 150-200 islets were seeded on each 12 mm coverslip for expansion. Islets were over-seeded to account for attrition during sample prep.

Expansion microscopy

We adapted our expansion protocol from the ultrastructure expansion microscopy (U-ExM) protocol developed by Paul Guichard Lab (Laporte et al. 2022), incorporating modifications by Jennifer Wang Lab at Washington University (gelation workflow, denaturing buffer recipe) (Langner et al. 2024), and Mu He Lab at Hong Kong University (coverslip stacks in gelation mold for 3D tissue expansion) (Chong et al. 2020).

Updated expansion workflow: A humidified gelation chamber was prepared using a 10 cm petri dish with a wet paper towel tucked around its inside perimeter. **Figure 1A** shows the pacement of sample slides and coverslips inside the gelation chamber. For 3D tissue expansion, two even stacks of square coverslips were used as buttresses to support the gelation mold to ensure uniform gel thickness. Two glass slides were used above and below the sample to ensure a smooth and clear surface on both sides of the gel. Gelation was performed using fresh-made gelation buffer (19% sodium acrylate, 10% acrylamide, 0.1% bis-acrylamide, 0.5% ammonium persulfate (APS), and 0.5% tetramethyl ethylenediamine (TEMED)), placed on top of seeded islets, and a glass slide was used as top cover. Samples were incubated at 4°C on ice for 5 minutes and then in a 37°C incubator for 45 minutes for monolayer cells and 1 hour for islet tissue. Denaturation was performed on solidified gels, freed from supporting slides and coverslips, and submerged in denaturation buffer (200 mM sodium dodecyl sulfate (SDS), 200 mM NaCl, 50 mM Tris-HCl pH 9) at 95°C for 1 hour. Expansion was performed by immersing the denatured gels in Milli-Q water, 30 minutes x 5 exchanges, total 150 minutes. Post-expansion samples could be stored in Milli-Q water or cut into small pieces and stored in PBS for up to 2 months. Of note, storage in PBS shrunk the gels by approximately 50% in diameter which required re-hydration and re-expansion using 2 x 30 minute exchanges in Milli-Q water before use.

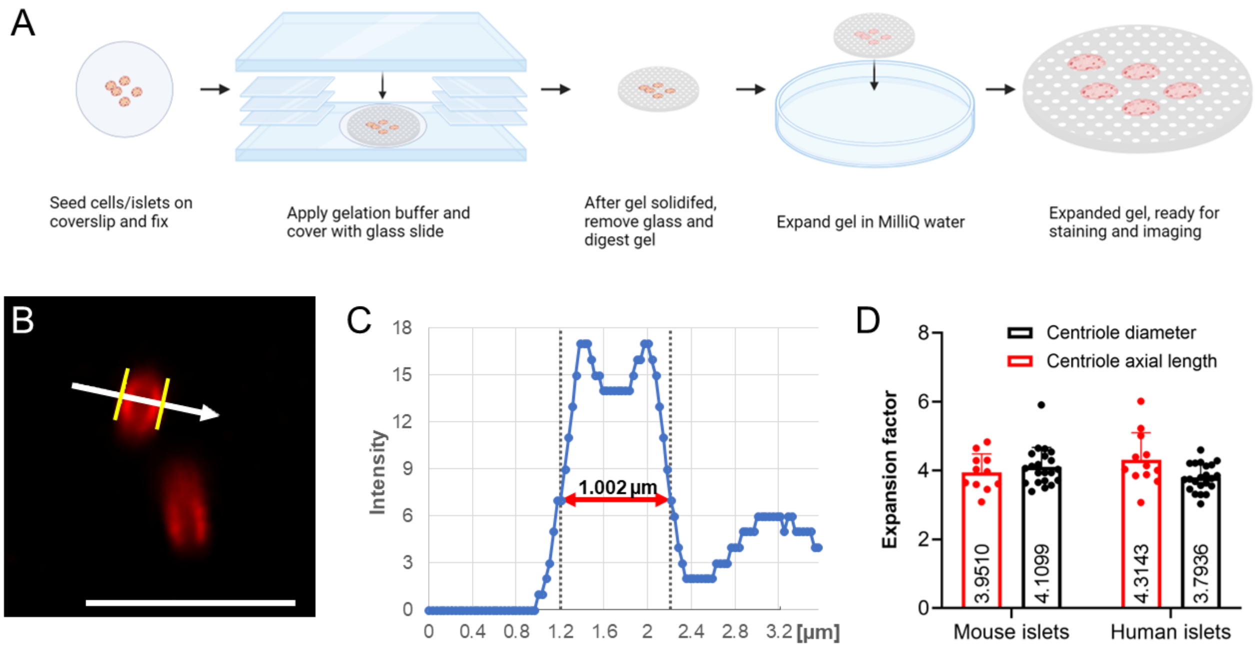

FIGURE 1. Workflow of ExM of pancreatic islets. (**A**) Optimized expansion workflow. Schematics are not to scale. (**B**) Centriolar measurement in Nikon NIS-Elements imaging software for expansion factor calculation. (**C**) Full width at half maximum (FWHM) measurements of expanded mouse islet centrioles, measuring 1 µm which corresponds to 4x expanded native centriole diameter of ~250 nm, scale 5 µm. (**D**) Expansion factor calculation results. n = 21-22 per centriole diameter measurement and n = 11-12 per centriole axial length measurement (p value: mouse diameter/axial = 0.8687; human diameter/axial = 0.0539; diameter mouse/human = 0.2541; axial mouse/human = 0.4058, all non-significant).

Immunostaining

Post-expansion gels were punched into 8 mm circular disks using the tops of P1000 pipette tips, then transferred to Eppendorf tubes for staining. Gels were first blocked in PBSBT (PBS with 3% bovine serum albumin (BSA), 0.1% Triton X-100, 0.02% sodium azide) for 30 minutes at room temperature, then incubated in primary antibodies diluted in PBSBT for 48 hours at 4°C. Samples were washed 5 times with PBSBT, 10 minutes each, then incubated with second antibodies and 4',6-diamidino-2-phenylindole (DAPI, 0.5 µg/mL) diluted in PBSBT overnight at 4°C. Stained samples were washed in Milli-Q water for 15 minutes x 5 times, then stored in Milli-Q water protected from light. Stained samples were imaged within two weeks of preparation.

Confocal microscopy and super-resolution microscopy

Immunofluorescence imaging was performed on a Zeiss LSM880 confocal microscope and a Nikon AXR super-resolution imaging system with Nikon spatial array confocal (NSPARC). Immunostained expanded gel samples were placed in a 35 mm glass-bottom dish coated with poly-D-lysine to minimize sample movement, and the gel sample surrounded with a wet paper towel to prevent gel drying and shrinkage. Imaging was performed using 20x, 60x, and 100x objectives to obtain a range of magnifications. Multichannel confocal images were acquired using manually fine-tuned emission bands on the LSM880 to minimize channel crosstalk, and using preset channel series on balanced mode on the Nikon AXR NSPARC, which acquired the red (561nm) and blue (450nm) channels together, while the green (488nm) channel was acquired separately to prevent red-green co-localization artifacts.

Expansion factor analysis

We used centriole size as a reference for calculating the expansion factor. The centriole is a well-characterized organelle by electron microscopy and commonly used as a molecular ruler for expansion factor analysis(Gambarotto et al. 2019; Sahabandu et al. 2019). We measured the diameter and axial length of expanded centrioles and compared them with the physical dimensions of nonexpanded centrioles. Only cells with centrioles that were fully captured by confocal imaging, with adequate side or section views, were selected for analysis.

Centriole diameter and axial length were measured using the Nikon NIS-Element built-in tool FWHM (Full Width at Half Maximum), a standard statistical measurement of an object's wave width at half its maximum value. An example of diameter measurement is shown in **Figure 1**, where an arrow is drawn perpendicularly through the centriole, crossing the center of section view (**Figure 1B**). The software quantifies the intensity of the image where the arrow passes and generates a trapezoid-shaped impulse wave for the centriole object (**Figure 1C**). The following formulas are then used for expansion factor calculation:

$$k_{Ed} = \frac{\sum_{i=1}^{n} d_i}{250n}$$

$$k_{El} = \frac{\sum_{j=1}^{m} d_j}{500m}$$

In these formulas, k_{Ed} represents the expansion factor of centriole diameter, and k_{El} represents the expansion factor of centriole axial length. n and m are the numbers of centrioles counted; d_i is the diameter of the ith centriole while d_j is the axial length of the jth centriole. Units for d_i and d_j are in nanometers (nm). The constant 250 derives from the average diameter of normal unexpanded centrioles which is ~250 nm (Uzbekov, Garanina, and Bressac 2018). The axial length of an unexpanded centriole varies depending on cell cycle status but typically falls within a broader range of 300 to 700 nm. Thus, the median length 500 nm is used here as a calculation constant for determining centriole length expansion factor.

Expansion factor analysis on expanded mouse and human islet samples showed ~4x expansion in both ratio of axial length and diameter (**Figure 1D**), indicating successful isotropic expansion. Expansion factor values were consistent among individual islet preparations and imaging experiments, attesting to the robustness and reproducibility of the ExM workflow. Similar expansion factors were identified between mouse and human islets ($p > 0.05$), indicating that our ExM protocol is suitable for islet samples across species.

Lentiviral knockdown

Dynein axonemal intermediate chain 1 (*Dnai1*) knockdown was performed in primary mouse islets using MISSION® lentiviral particles (Sigma Clone ID: TRCN0000115519 (shDNAI1-1), TRCN0000115517 (shDNAI1-2), SHCLNV). Control knockdown was MISSON® pLKO.1-puro non-target shRNA (Sigma, SHC016VN-1EA). For optimal transduction efficiency, mouse pancreatic islets required a brief and partial dissociation step using Accutase (Innovative Cell technologies AT-104) for 5 minutes x 2 times at 37°C in Eppendorf tubes. A minimum of 50 islets were used per knockdown condition. Partially dissociated islets were transduced with either control or *Dnai1* shRNA lentiviral particles in polybrene (10 µg/mL) at 5 x 10^5 viral particles/mL for 24 hours at 37°C (Jimenez-Moreno et al., 2015). Post-shRNA transduction, islets were recovered and reaggregated in a 12-well low-cell attachment plate (Thermo Fisher Scientific, 174931) for 96 hours, before using for immunostaining and gene expression experiments.

Quantitative polymerase chain reaction (qPCR)

shRNA knockdown efficiency was validated by qPCR. Total mRNA was isolated from transduced and re-aggregated mouse islet cells by lysing in 350 µL of lysis buffer RA1 (Macherey-Nagel, 740961) with β-mercaptoethanol. RNA was purified using the Nucleospin RNA kit (Macherey-Nagel, 740955.50), and complementary DNA (cDNA) was synthesized with High-Capacity cDNA reverse transcription kit (Thermo Fisher Scientific, 4368814). Quantitative PCR was performed in triplicate on a QuantStudio 3 Real-Time PCR Instrument (Thermo Fisher Scientific, A28131) using 2x Power SYBR Green PCR Master Mix (Thermo Fisher Scientific, 4367659). Gene expression levels were quantified using $2^{-\Delta\Delta Ct}$ and normalized by the housekeeping gene *Gapdh*. The following primer sequences were used: mouse *Dnai1*: F: 5’-ACCTCCAAGTCTGGCAAGCACA-3', R: 5’-ACTATCCTGCCATCGGACGACA-3'; mouse *Gapdh*: F: 5’- AGGTTGTCTCCTGCGACTTCA-3', R: 5’-CAGGAAATGAGCTTGACAAAGTTG-3'.

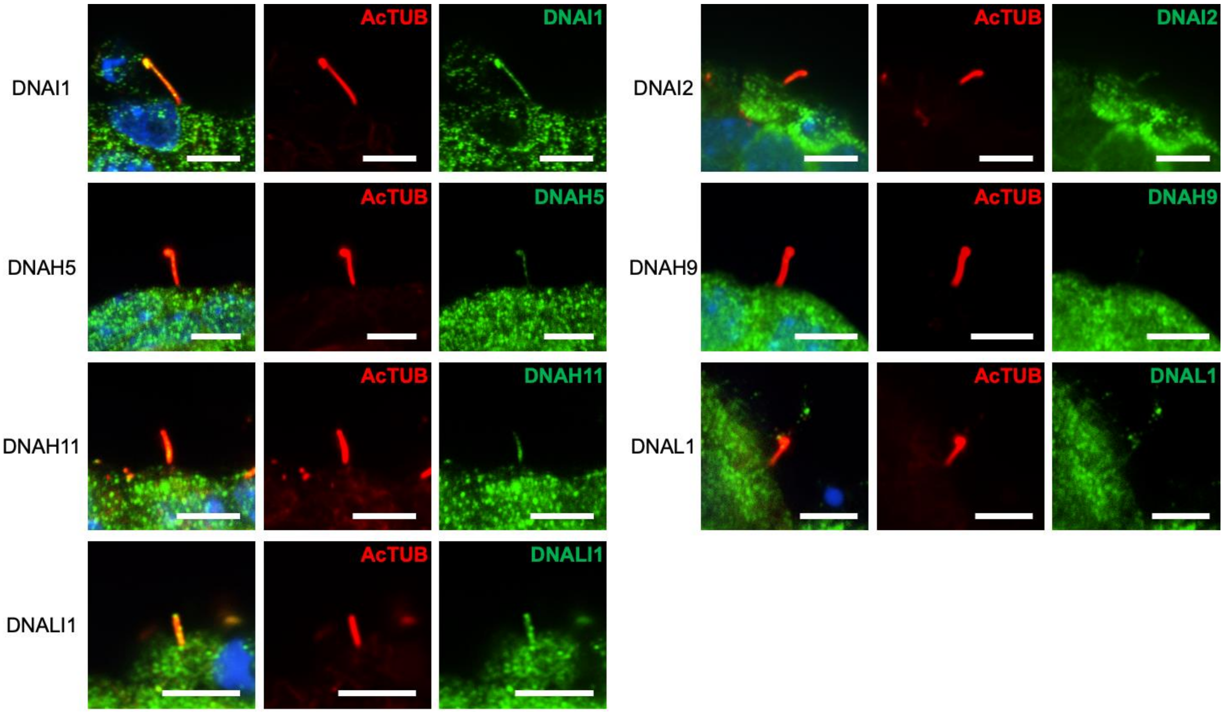

FIGURE 2. Axonemal dynein expression in unexpanded mouse islets. Antibody and IF protocol validation showing ciliary localization of 7 different axonemal dynein components in native unexpanded wild-type mouse islets. Representative collages are shown for each dynein subunit (green), acetylated alpha-tubulin (AcTUB, red), and merged (nuclei, DAPI, blue); scale 5 µm. All 7 axonemal dyneins were detected in mouse islet cilia, including DNAI1, DNAH5, DNAH11, and DNALI1 (left column) which exhibited strong ciliary labeling, and DNAI2, DNAH9, and DNAL1 (right column) which had relatively weaker ciliary staining. All 7 dyneins were tested in downstream ExM.

RESULTS

Antibody validation for axonemal dynein staining in mouse primary cilia

We have previously reported successful axonemal dynein staining in human islet primary cilia (Cho et al. 2022), while the demonstration of ciliary dyneins in primary mouse tissue has been more challenging due to antibody performance variability. Here, using a standardized sample preparation and staining protocol, we tested a panel of 7 commercial rabbit polyclonal antibodies to axonemal dynein subunits in mouse pancreatic islets, including dynein axonemal intermediate chain 1 (DNAI1), intermediate chain 2 (DNAI2), heavy chain 5 (DNAH5), heavy chain 9 (DNAH9), heavy chain 11 (DNAH11), light chain 1 (DNAL1), and light intermediate chain 1 (DNALI1) (**Table 1**). All 7 dynein subunits were detectable in native unexpanded mouse islet cilia, shown in the green channel in **Figure 2**, with variable labeling intensities referenced against a red cilia/centriole channel (acetylated alpha tubulin, AcTUB). Consistently, using our IF protocol, DNAI1, H5, H11, and LI1 antibodies produced strong colocalization with AcTUB, indicating ciliary expression of the proteins, while the ciliary signals of DNAI2, H9, and L1 were less robust.

As most dynein antibodies produced cytoplasmic staining signals, we validated antibody specificity using targeted shRNA knockdown against DNAI1, the strongest staining dynein based on our preliminary results. We performed *Dnai1* knockdown in mouse islets using two independent lentiviral constructs (**Figure 3A**). Quantitative PCR showed 63-68% reduction in *Dnai1* mRNA compared to scrambled control, while imaging quantitation of ciliary DNAI1 protein confirmed knockdown-specific reduction of DNAI1 fluorescence intensity, both in the cytoplasm and in the primary cilium as normalized to ciliary AcTUB signal (**Figure 3B-C**). Collectively, these results validate the robustness of our DNAI1 immunostaining and the antigen specificity of the DNAI1 antibody.

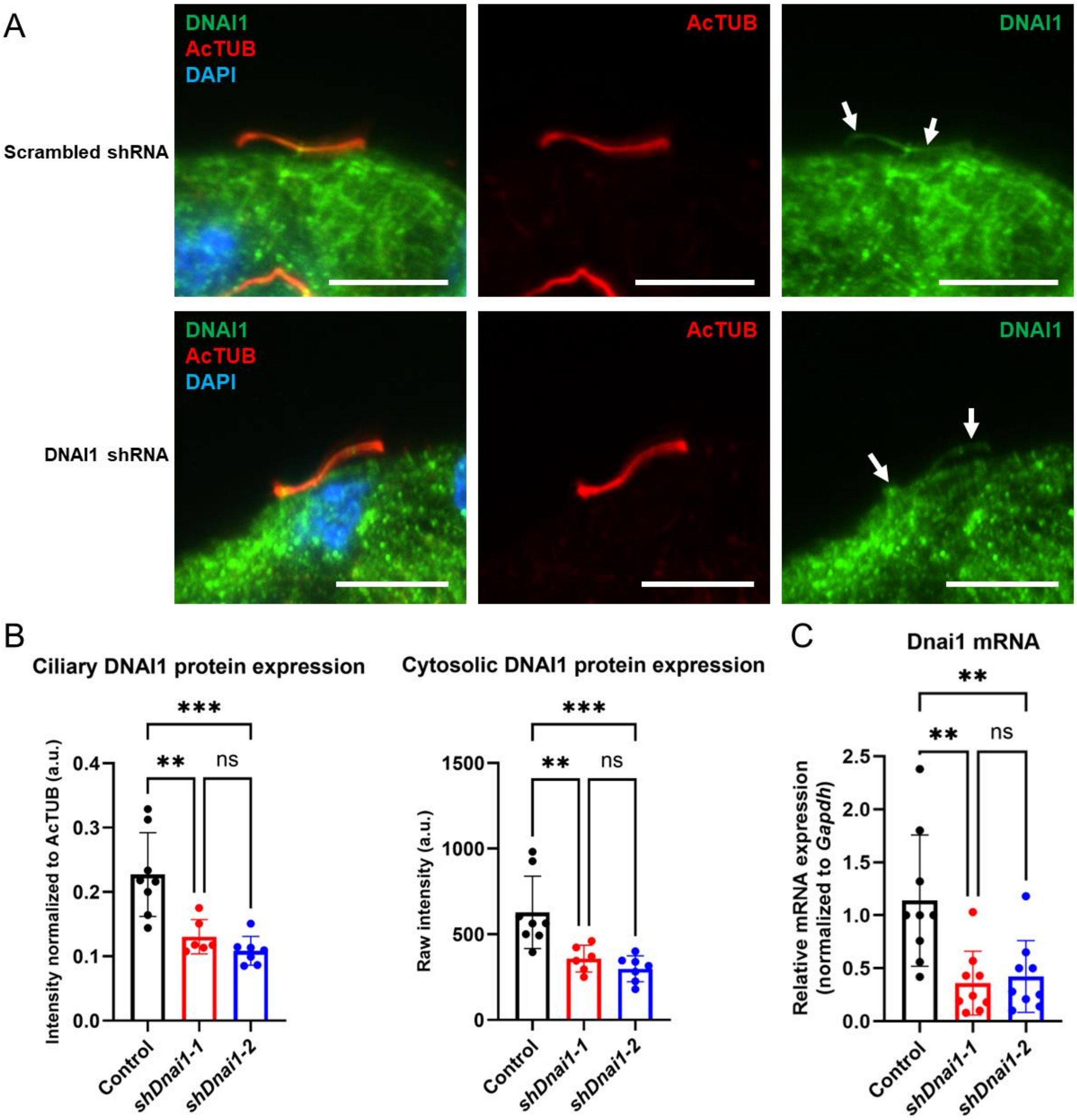

FIGURE 3. DNAI1 staining validation by lentiviral knockdown. Two independent lentiviral shRNA knockdowns of DNAI1 were performed in control wild type mouse islets, showing diminished DNAI1 staining in KD compared to control islets. (A) Control scrambled shRNA (top row) showing DNAI1 expression in mouse islet cilia (white arrows) as marked by acetylated alpha-tubulin (AcTUB, red). DNAI1 shRNA (bottom row) led to reduced dynein staining. Nuclei, DAPI (blue); scale 5 μm. (B) Normalized immunofluorescent signal intensity of ciliary DNAI1 protein staining (left panel) and overall cytosolic DNAI1 intensity (right panel) are both diminished following shRNA knockdown using two lentiviral Dnai1 constructs, n = 6-8 islets quantitated per knockdown condition. The knockdown efficiency of the ciliary proteins is 43% and 52%

for the two shRNA constructs, and the cytosolic proteins show similar knockdown efficiencies of 43% and 52%, respectively. One-way ANOVA, $^{**}p < 0.01$, $^{***}p < 0.001$, ns, not significant. (C) qPCR showing successful Dnai1 knockdown using two independent lentiviral shRNA constructs, which achieved knockdown efficiencies of 68% and 63%, respectively. Dnai1 knockdown cDNA samples loaded in triplicate were individually normalized by controls. n = 9 per knockdown condition. One-way ANOVA, $^{**}p < 0.01$; ns, not significant.

Application of ExM to MIN6 beta cells and mouse islets

To increase the spatial resolution in our ciliary protein localizations, we applied ExM to physically expand beta cells and their cilia in an embedded hydrogel prior to confocal imaging. We first did proof-of-concept testing on cultured MIN6 beta cells, a murine insulinoma cell line that shares morphological and physiological features with primary beta cells including cilia expression and glucose-responsive insulin secretion. We compared primary cilia morphology between images acquired from unexpanded and expanded samples and used empiric measurements to calculate the expansion factor and to validate expansion efficiency. Both primary cilia (AcTUB, red) and centrioles (FOP, green) were detected in unexpanded and expanded MIN6 beta cells (**Figure 4A**). Centrioles in unexpanded cells appeared as a single or pair of green dots, while centrioles in expanded cells were resolvable as orthogonally positioned barrels, with sharp, crisp edges and an annular cross-section (green channel, boxed insets, mid and right panels, **Figure 4A**). Similarly, the ciliary axoneme as labeled by acetylated alpha-tubulin (AcTUB, red channel, mid and right panels, **Figure 4A**) showed greater structural detail in expanded samples, with bright uniform AcTUB labeling along the length of the axoneme. These results show that ExM provides superior detail in visualizing primary cilia and centrioles in mouse beta cells.

Building on MIN6 cell results, we applied ExM to primary cilia imaging in intact murine islet tissue. Mouse islet cells each expressed a primary cilium which was readily detectable by AcTUB staining (**Figure 4B**). Axonemal dynein (DNAI1, green) co-staining labeled punctate structures in the cytosol and in cilia, seen clearly in projecting cilia at the islet periphery (**Figure 4B**, left panel). Expansion produced superior resolution of the axonemal microtubule filaments (**Figure 4B**, mid and right panels), which were previously unresolvable in native unexpanded samples. DNAI1 staining exhibited a discrete punctate distribution along the microtubule tracks, which on cross-sectional view was seen as associating with each microtubule filament in a ring-like symmetry around the axoneme (**Figure 4B**, right panel).

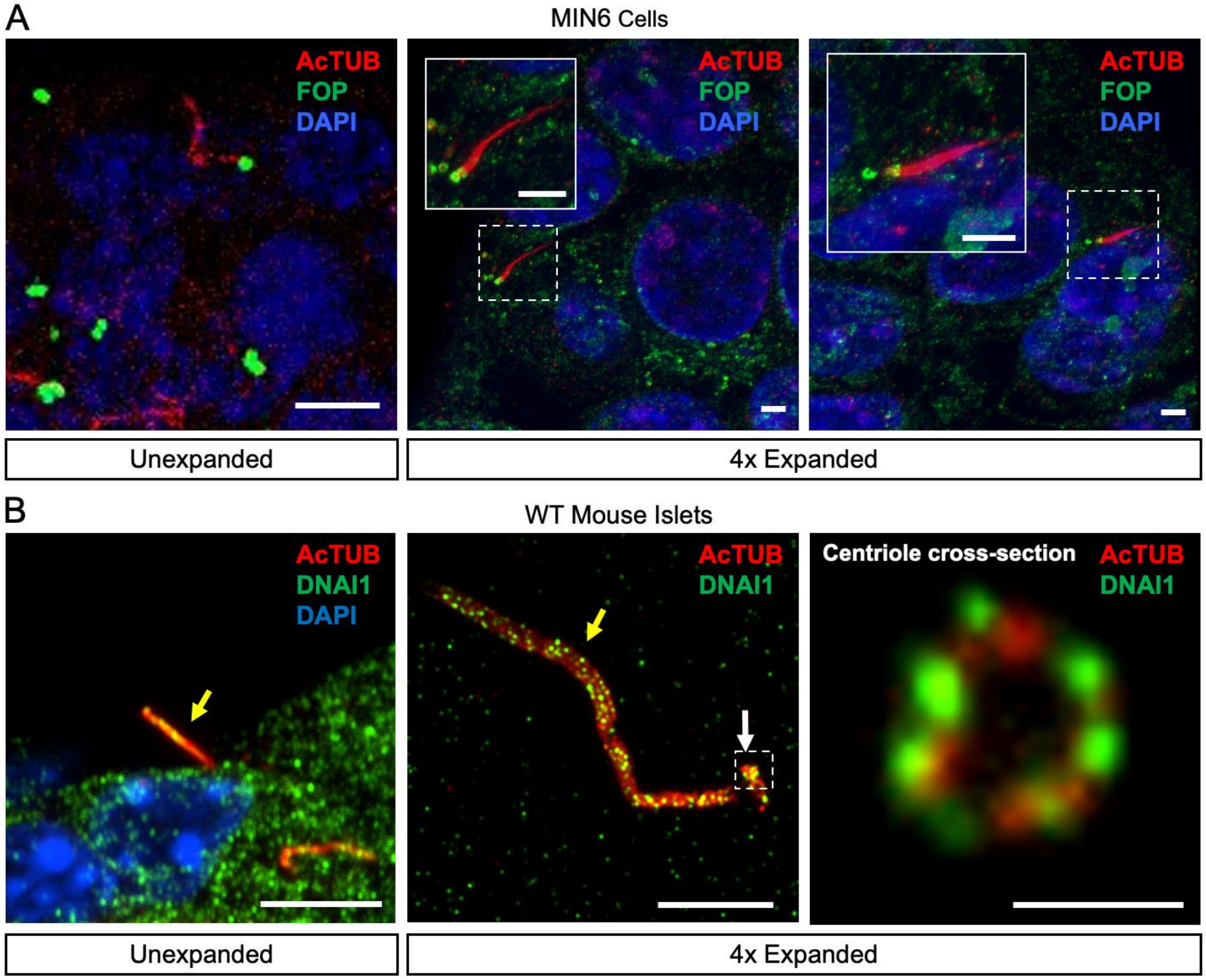
A
MIN6 Cells
AcTUB
FOP
DAPI
Unexpanded
4x Expanded
B
WT Mouse Islets
AcTUB
DNAI1
DAPI
Centriole cross-section
Unexpanded
4x Expanded

FIGURE 4. Primary cilia ExM in mouse MIN6 beta cells and islets by conventional confocal and super-resolution microscopy. (**A**) LSM 880 confocal microscope images of native unexpanded and expanded MIN6 beta cells, showing preserved ciliary and cytomorphology after the expansion process. Cells are co-labeled with axoneme marker acetylated alpha-tubulin (AcTUB, red), centriole marker FGFR1 oncogene partner (FOP, green), and nuclei (DAPI, blue). Insets (solid-borders) are enlarged from dashed-border regions to show details, scale 5 µm. (**B**) Nikon AXR NSPARC microscope images of WT mouse islets acquired on super-resolution mode, showing preservation of cilia morphology and improved resolution of ciliary dynein (DNAI1, green) detection after expansion. Left and mid panels: ciliary axoneme, yellow arrows; centriole, white arrow; scale 5 µm. Right panel: *en face* view of the centriole cross-section, showing ring-like distribution of DNAI1 (green) in association with AcTUB (red)-staining microtubule filaments, scale 1 µm.

Improved ExM workflow captures greater detail in 3D islet cilia imaging

The main methodological modification we introduced into the ExM workflow was adding physical supports in the gelation mold to promote uniform gelation of 3D islet samples. After initially running into problems with uneven expansion and distorted islet morphology using unsupported coverslips as a lid for gelation (depicted in **Figure 5A-B**, left panels), we modified the setup to include a) seeding islets first onto a small, 12 mm diameter, round coverslip (Platinum Line® #1,5) before applying gelation solution, which made the gels smaller, easier to handle, with more uniform surface flatness, and b) a pair of stacked glass coverslips on two sides of the sample, buttressing the gelation mold and allowing whole islets to be fully embedded in an even-thickness gel (**Figure 5A**, right panel). We used 3 x 0.15 mm thickness coverslips with a net vertical gap of 0.3 mm (minus the thickness of the bottom coverslip on which islets were seeded), which provided sufficient z-distance to embed mouse islets that averaged 100-250 µm in diameter. The resultant gels minimized deformation of primary cilia and cell body caused by external pressure of the glass slides above and below in the traditional gelation protocol (**Figure 5A-B**, left panels), and enabled superior volumetric expansion and preservation of cytomorphological structures (**Figure 5A-B**, right panels). This updated ExM workflow allowed reproducible results in expansion and imaging. We were able to observe larger numbers of cilia that were preserved in their native full-length state (**Figure 5B**, right panel), with clearly distinguishable axoneme and centrioles, and compelling images of AcTUB and DNAI1 co-localization (**Figure 5C**).

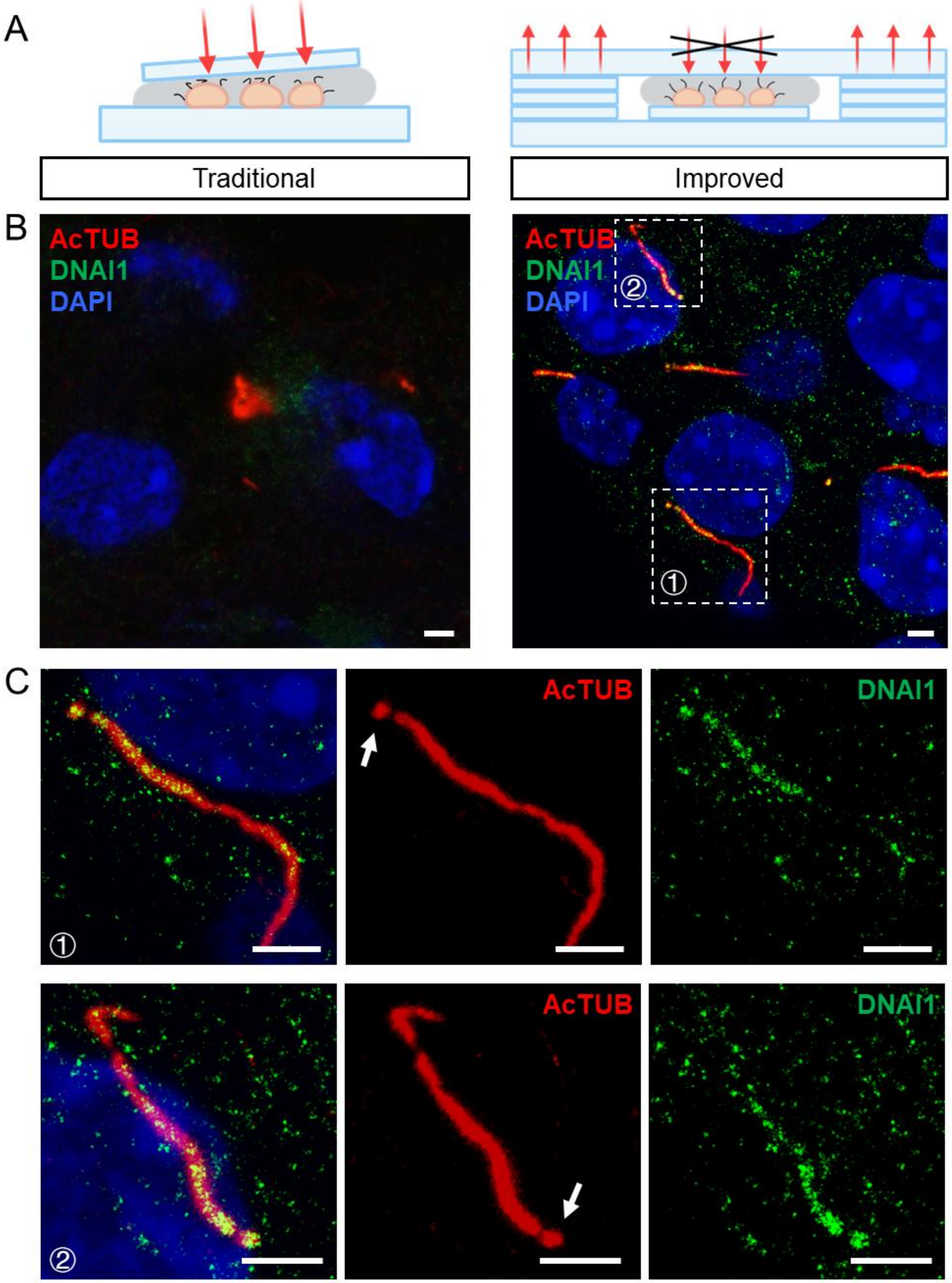
A
Traditional
Improved
B
AcTUB
DNAI1
DAPI
AcTUB
DNAI1
DAPI
②
①
C
①
AcTUB
DNAI1
②
AcTUB
DNAI1

FIGURE 5. ExM optimization for ciliary detection in intact mouse islet tissue. (**A**) Schematic illustration of an improved gelation setup using stacked coverslips as buttresses, allowing for even thickness of the gel and uniform pressure from the top glass slide. (**B**) Representative 8-µm z-projections of mouse islets imaged on a Zeiss LSM 880 confocal microscope comparing traditional versus improved expansion protocol. The traditional protocol produced uneven expansion with distorted nuclei and cilia, whereas cytomorphologic features were better preserved in the improved protocol. scale, 5 µm. (**C**) High magnification images of inset regions in (**B**), showing two cilia co-labeled by acetylated alpha-tubulin (AcTUB, red) and axonemal dyneins (DNAI1, green); white arrows denote centrioles at the ciliary base, scale 5 µm.

Expansion microscopy detects axonemal dyneins on islet primary cilia

The biological question that drives our ExM studies is to provide definitive evidence of axonemal dynein expression and distribution in islet cilia. We did this in both mouse and human islets, testing the hypothesis that ExM would enable resolution of sub-ciliary dynein expression patterns. Of the seven dynein antibodies that we validated in nonexpanded mouse samples in **Figure 2**, four dyneins including DNAI1, H5, H11, and LI1 showed definitive ciliary staining in expanded mouse islets as indicated by overlapping signals with axonemal AcTUB (**Figure 6**). Three other dyneins, DNAI2, H9, and L1, did not produce definitive ciliary staining in expanded islets (not shown). Of the four dynein antibodies that did produce ciliary signals, DNAI1 and DNAH5 labeled the ciliary axoneme strongly and continuously from base to tip (**Figure 6A-B**), similar to their labeling patterns in nonexpanded mouse islets. DNAH11 in expanded mouse islets recapitulated strong expression in the proximal axoneme, concentrating at the ciliary base and transition zone (**Figure 6C**). DNALI1 was detected in the axoneme, with discrete punctate staining in association with the axonemal microtubules as labeled by AcTUB (**Figure 6D**). These results indicate that different dynein subunits may have different spatial distribution within the islet primary cilium.

ExM of human islets revealed similar dynein localization patterns as in mouse islets. Ciliary expressions of DNAI1, H5, H11, and LI1 were detected in healthy human islets, with DNAI1 strongly labeling the full-length axoneme and centriole (**Figure 7A**), DNAH5 labeling parts of the axoneme and centrioles (**Figure 7B**), DNAH11 labeling the cilia base (**Figure 7C**), and DNALI1 sparsely labeling the axoneme in punctate form (**Figure 7D**). Of these four dyneins, DNAH5 staining had the lowest signal-to-noise ratio due to higher background, which may have been due to relatively greater cytosolic DNAH5 expression or non-specific binding by the antibody. DNALI1 antibody produced somewhat higher background staining in human islets compared to mouse islets consistently across experiments, likely reflecting greater nonspecific binding of this antibody in human islet tissue. In both human and mouse islets, the distinct sub-ciliary distribution pattern of each axonemal dynein indicates possible specialization of their roles in promoting cilia motility, assembly, and function.

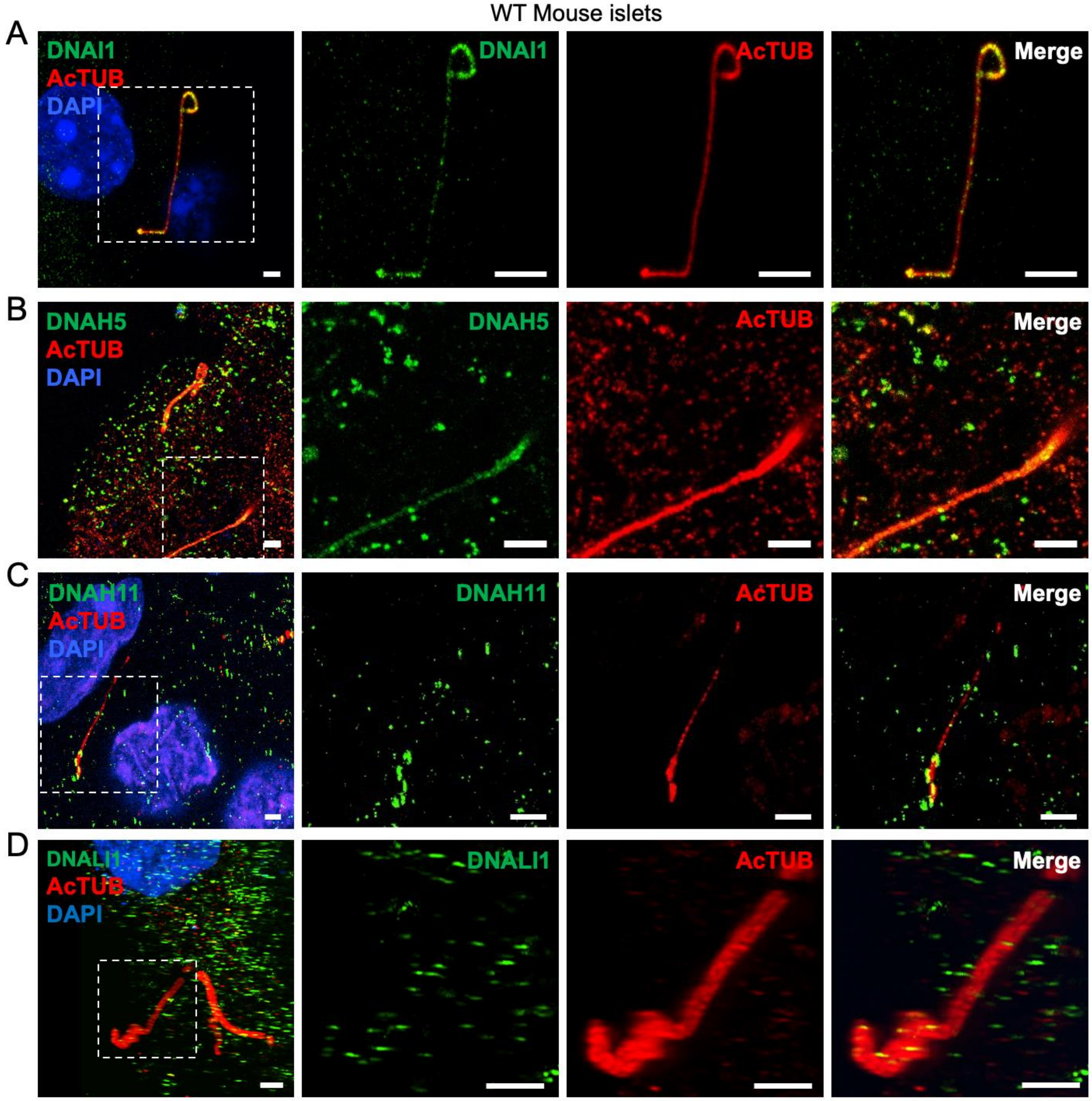
WT Mouse islets
A
DNAI1
AcTUB
DAPI
DNAI1
AcTUB
Merge
B
DNAH5
AcTUB
DAPI
DNAH5
AcTUB
Merge
C
DNAH11
AcTUB
DAPI
DNAH11
AcTUB
Merge
D
DNALI1
AcTUB
DAPI
DNALI1
AcTUB
Merge

FIGURE 6. Super-resolution imaging of axonemal dynein in expanded mouse islets. Expanded wild-type mouse islets labeled with axonemal dynein isoforms and imaged on a Nikon AXR microscope. Left-side panels show a low-magnification view; right-side panels show magnified insets in single-channel and merge views. **(A)** Dynein axonemal intermediate chain 1 (DNAI1, green) strongly labels the ciliary axoneme from base to tip. **(B)** DNAH5 strongly labels the full-length axoneme in mouse islet cilia. **(C)** DNAH11 expression in mouse islets is concentrated at the cilia base. **(D)** DNALI1 localizing to the tortuous tip of a primary cilium. Cilia marker, acetylated alpha-tubulin (AcTUB, red), scale 5 μm.

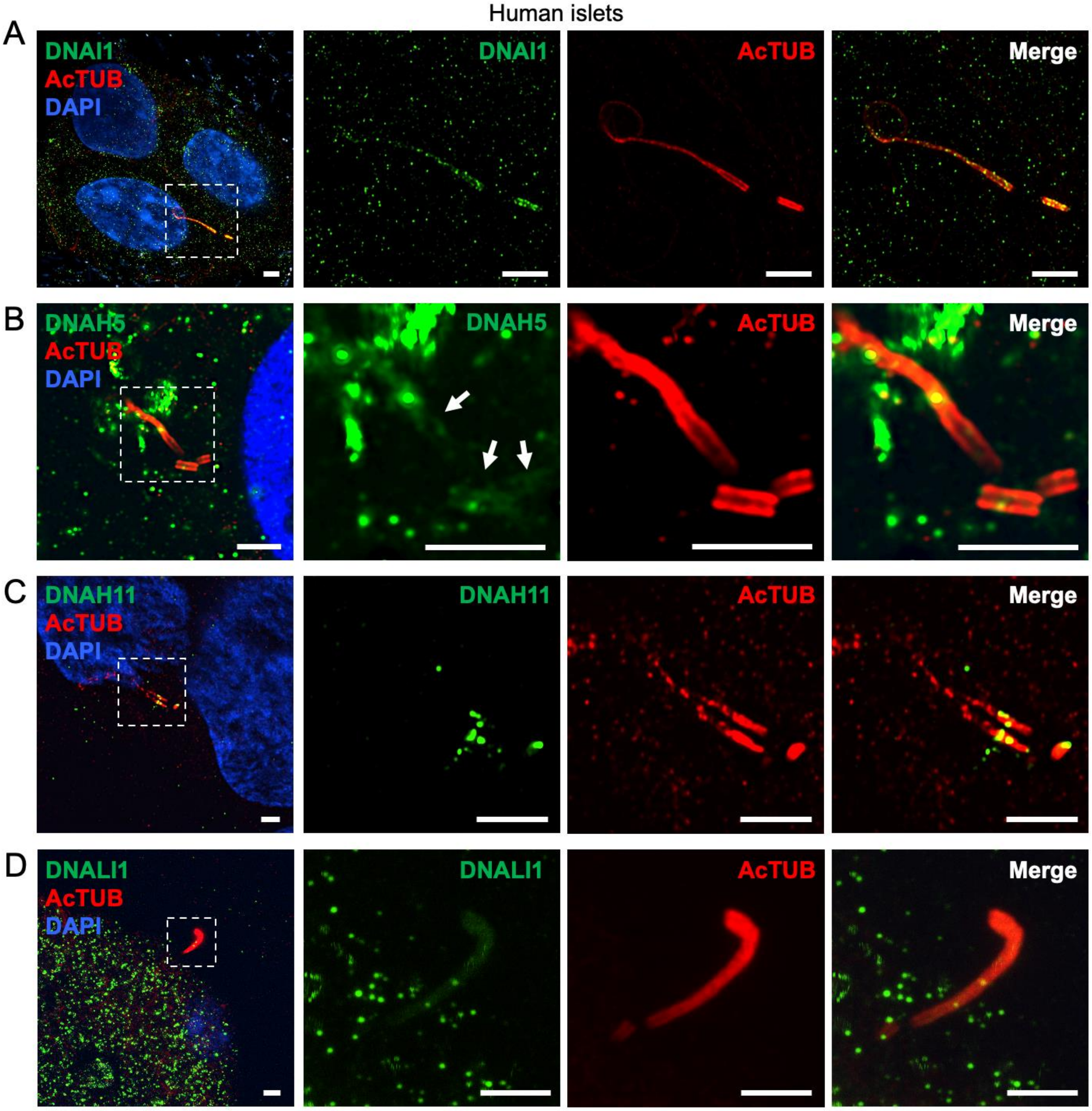
Human islets
A
DNAI1
AcTUB
DAPI
DNAI1
AcTUB
Merge
B
DNAH5
AcTUB
DAPI
DNAH5
AcTUB
Merge
C
DNAH11
AcTUB
DAPI
DNAH11
AcTUB
Merge
D
DNALI1
AcTUB
DAPI
DNALI1
AcTUB
Merge

FIGURE 7. Super-resolution imaging of human islet cilia showing axonemal dynein expression. ExM-expanded islets from healthy human donors exhibit ciliary and centriolar expression of axonemal dyneins, including **(A)** DNAI1, **(B)** DNAH5 (white arrows), **(C)** DNAH11, and **(D)** DNALI1. Cytoplasmic expressions of DNAI1, DNAH5, and DNALI1 are also seen. Dynein (green), acetylated alpha-tubulin (AcTUB, red), nuclei (DAPI, blue), scale 5 µm.

DISCUSSION

We show here that 3D expansion microscopy (ExM) can be used to map dynein protein expression on primary cilia in pancreatic islets. Following validation of the ExM technique using MIN6 beta cells, we applied ExM to imaging cilia in primary mouse and human islets. Our results show that ExM is a useful approach for enabling nanoscale imaging of densely packed tissues and for resolving small subcellular structures that may otherwise be inaccessible to conventional light fluorescence microscopy. The main methodological innovation in our ExM protocol was a small redesign in the gelation chamber to produce more uniform gel samples. By reducing the external pressure exerted on the islets during gelation, we minimized sample distortion to achieve more isotropic expansion of the tissue samples, allowing faithful recapitulation of 3D islet cytomorphology and increased confidence in cilia localization data. The ability to image the expanded samples on conventional confocal microscopes and achieve sub-micron detail meant greater flexibility in choosing imaging equipment and making super-resolution cilia imaging more accessible.

We did encounter several limitations in the ExM workflow worth noting and improving in future work: 1) Antibody performance: of the 7 dynein antibodies that demonstrated ciliary labeling in native unexpanded mouse islets, 3 lost their ciliary signals after ExM, suggesting that certain antibodies may not perform rigorously across sample preparation protocols, and that antigenic epitopes may be lost from the denaturing or physical expansion process. 2) Low signal-to-noise: axonemal dynein proteins and primary cilia are both low-abundance targets for imaging, countered against the heavy background in the cytosol, which sometimes precluded interpretation of ciliary signals and reduced the number of usable images. To mitigate this, we focused on imaging protruding cilia on the islet periphery where the background is relatively clear. We also used shRNA knockdown to validate DNAI1 staining, which increased confidence in the specificity of the observed ciliary labeling. We also considered isolating cilia from the cell body using a calcium shock protocol (Ishikawa and Marshall 2013), but opted not to proceed to preserve the intact cilia structure. 3) Sample preparation cost: ExM is an antibody-costly procedure. During early stages of protocol optimization, we had compared pre- versus post-expansion labeling, the rationale being that pre-expansion labeling on a smaller piece of gel would help conserve antibody. However, the pre-expansion staining did not survive expansion. Thus, using exclusively post-expansion labeling in this work, we used an estimated 500 µL of each primary antibody for a total of 200 gel punches each for mouse and human islet samples (antibodies purchased at standard 50-100 µg/µL concentration, used at 1:100-400 dilution). We also found that storing post-expansion, stained gels in ddH2O led to fading of fluorescent signals after 2 weeks, limiting the ability to re-image samples. Future experiments might incorporate sample preservation steps e.g. post-fix or storing in a mounting buffer to protect fluorophores and prolong sample usability.

In summary, we optimize and apply an ExM protocol to identify axonemal dynein subunits in the primary cilia of 3D pancreatic islet tissue. The expansion sample preparation and imaging protocol is robust, producing consistent results in mouse and human islet tissues. The observation of multiple protein subunits of axonemal dynein in islet primary cilia, and their conservation across species, suggesting a functional role for dynein motors in islet primary cilia. Future work might further improve this ExM workflow to incorporate larger tissue volumes e.g. pancreatic slices, combine iterative expansion and super-resolution modalities to achieve even greater imaging resolution, and mechanistically explore the functional relevance of axonemal dynein action in islet primary cilia and in other cellular contexts.

ACKNOWLEDGEMENT

We thank Drs. Jenn Wang and Mu He for ExM protocol sharing and technical assistance and the WashU Cilia & Centrosome group for helpful discussion. Microscopy was performed at the Washington University Center for Cellular Imaging (WUCCI) supported by Washington University School of Medicine, The Children's Discovery Institute of Washington University and St. Louis Children's Hospital (CDI-CORE-2015-505 and CDI-CORE-2019-813) and the Foundation for Barnes-Jewish Hospital (3770 and 4642). Graphical illustrations created with BioRender. Funding for this study provided by NIH grants R01DK138974 and R01DK140365 to JWH.

TABLE 1. Antibody source, dilution, and performance

Antibody	Source	Product #	Dilution	Performance
Cilia & centriole markers				
AcTUB mouse monoclonal IgG2b	Sigma	T7451	1:200	Excellent
FGFR1OP rabbit polyclonal	Proteintech	11343-1-AP	1:500	Excellent
Axonemal dyneins				
DNAI1 rabbit polyclonal	Sigma	HPA021649	1:200	Good
DNAI2 rabbit polyclonal	Proteintech	17533-1-AP	1:200	Poor
DNAH5 rabbit polyclonal	Sigma	HPA037469	1:100	Fair
DNAH9 rabbit polyclonal	Invitrogen	PA5-45744	1:100	Poor
DNAH11 rabbit polyclonal	Sigma	HPA056474	1:400	Fair
DNAL1 rabbit polyclonal	Sigma	HPA053129	1:400	Poor
DNALI1 rabbit polyclonal	Proteintech	17601-1-AP	1:400	Fair
Secondary antibodies				
Alexa Fluor 568 goat anti-mouse IgG2b	Invitrogen	A21144	1:500	Excellent
Alexa Fluor 488 goat anti-rabbit IgG (H+L)	Invitrogen	A11008	1:500	Excellent

REFERENCES

Cheng, Kim, Viviane Delghingaro-Augusto, Christopher J. Nolan, Nigel Turner, Nicole Hallahan, Sofianos Andrikopoulos, and Jenny E. Gunton. 2012. “High Passage MIN6 Cells Have Impaired Insulin Secretion with Impaired Glucose and Lipid Oxidation.” *PLoS ONE* 7(7):e40868. doi: 10.1371/journal.pone.0040868.

Cho, Jung Hoon, Zipeng A. Li, Lifei Zhu, Brian D. Muegge, Henry F. Roseman, Eun Young Lee, Toby Utterback, Louis G. Woodhams, Philip V. Bayly, and Jing W. Hughes. 2022. “Islet Primary Cilia Motility Controls Insulin Secretion.” Science Advances 8(38):eabq8486. doi: 10.1126/sciadv.abq8486.

Chong, Weng Man, Won-Jing Wang, Chien-Hui Lo, Tzu-Yuan Chiu, Ting-Jui Chang, You-Pi Liu, Barbara Tanos, Gregory Mazo, Meng-Fu Bryan Tsou, Wann-Neng Jane, T. Tony Yang, and Jung-Chi Liao. 2020. “Super-Resolution Microscopy Reveals Coupling between Mammalian Centriole Subdistal Appendages and Distal Appendages” edited by A. Akhmanova and L. Pelletier. eLife 9:e53580. doi: 10.7554/eLife.53580.

Gambarotto, Davide, Fabian U. Zwettler, Maeva Le Guennec, Marketa Schmidt-Cernohorska, Denis Fortun, Susanne Borgers, Jörn Heine, Jan-Gero Schloetel, Matthias Reuss, Michael Unser, Edward S. Boyden, Markus Sauer, Virginie Hamel, and Paul Guichard. 2019. “Imaging Cellular Ultrastructures Using Expansion Microscopy (U-ExM).” Nature Methods 16(1):71–74. doi: 10.1038/s41592-018-0238-1.

Hohmeier, Hans E., and Christopher B. Newgard. 2004. “Cell Lines Derived from Pancreatic Islets.” Molecular and Cellular Endocrinology 228(1):121–28. doi: 10.1016/j.mce.2004.04.017.

Hughes, Jing W., Jung Hoon Cho, Hannah E. Conway, Michael R. DiGruccio, Xue Wen Ng, Henry F. Roseman, Damien Abreu, Fumihiko Urano, and David W. Piston. 2020. “Primary Cilia Control Glucose Homeostasis via Islet Paracrine Interactions.” Proceedings of the National Academy of Sciences of the United States of America 117(16):8912–23. doi: 10.1073/pnas.2001936117.

Ishikawa, Hiroaki, and Wallace F. Marshall. 2013. “Chapter Fifteen - Isolation of Mammalian Primary Cilia.” Pp. 311–25 in Methods in Enzymology. Vol. 525, Cilia, Part B, edited by W. F. Marshall. Academic Press.

Klena Nikolai, and Pigino Gaia. 2022. “Structural Biology of Cilia and Intraflagellar Transport.” Annual Review of Cell and Developmental Biology 38(Volume 38, 2022):103–23. doi: 10.1146/annurev-cellbio-120219-034238.

Lacy, Paul E., and Mery Kostianovsky. 1967. “Method for the Isolation of Intact Islets of Langerhans from the Rat Pancreas.” Diabetes 16(1):35–39. doi: 10.2337/diab.16.1.35.

Langner, Ewa, Pongpratch Puapatanakul, Rachel Pudlowski, Dema Yaseen Alsabbagh, Jeffrey H. Miner, Amjad Horani, Susan K. Dutcher, Steven L. Brody, Jennifer T. Wang, Hani Y. Suleiman, and Moe R. Mahjoub. 2024. “Ultrastructure Expansion Microscopy (U-ExM) of Mouse and Human Kidneys for Analysis of Subcellular Structures.”

Laporte, Marine H., Nikolai Klena, Virginie Hamel, and Paul Guichard. 2022. “Visualizing the Native Cellular Organization by Coupling Cryofixation with Expansion Microscopy (Cryo-ExM).” Nature Methods 19(2):216–22. doi: 10.1038/s41592-021-01356-4.

Li, Dong-Sheng, Ya-Hong Yuan, Han-Jun Tu, Qing-Le Liang, and Long-Jun Dai. 2009. “A Protocol for Islet Isolation from Mouse Pancreas.” Nature Protocols 4(11):1649–52. doi: 10.1038/nprot.2009.150.

Li, Zipeng A., Jung Hoon Cho, Louis G. Woodhams, and Jing W. Hughes. 2022. “Fluorescence Imaging of Beta Cell Primary Cilia.” Frontiers in Endocrinology 13. doi: 10.3389/fendo.2022.1004136.

Müller, Andreas, Nikolai Klena, Song Pang, Leticia Elizabeth Galicia Garcia, Davud Sulaymankhil, Oleksandra Topcheva, Monika Seliskar, Hassan Mziaut, Eyke Schöniger, Daniela Friedland, Nicole Kipke, Susanne Kretschmar, Carla Münster, Jürgen Weitz, Marius Distler, Thomas Kurth, Deborah Schmidt, Harald F. Hess, C. Shan Xu, Gaia Pigino, and Michele Solimena. 2023. Structure, Interaction, and Nervous Connectivity of Beta Cell Primary Cilia. preprint. Cell Biology. doi: 10.1101/2023.12.01.568979.

Nakashima, Koji, Yukiko Kanda, Yasushi Hirokawa, Fumiko Kawasaki, Michihiro Matsuki, and Kohei Kaku. 2009. “MIN6 Is Not a Pure Beta Cell Line but a Mixed Cell Line with Other Pancreatic Endocrine Hormones.” Endocrine Journal 56(1):45–53. doi: 10.1507/endocrj.K08E-172.

Phelps, Edward A., Chiara Cianciaruso, Jaime Santo-Domingo, Miriella Pasquier, Gabriele Galliverti, Lorenzo Piemonti, Ekaterine Berishvili, Olivier Burri, Andreas Wiederkehr, Jeffrey A. Hubbell, and Steinunn Baekkeskov. 2017. “Advances in Pancreatic Islet Monolayer Culture on Glass Surfaces Enable Super-Resolution Microscopy and Insights into Beta Cell Ciliogenesis and Proliferation.” Scientific Reports 7(1):45961. doi: 10.1038/srep45961.

Polino, Alexander J., Sanja Sviben, Isabella Melena, David W. Piston, and Jing W. Hughes. 2023. “Scanning Electron Microscopy of Human Islet Cilia.” Proceedings of the National Academy of Sciences 120(22):e2302624120. doi: 10.1073/pnas.2302624120.

Reck-Peterson, Samara L., William B. Redwine, Ronald D. Vale, and Andrew P. Carter. 2018. “The Cytoplasmic Dynein Transport Machinery and Its Many Cargoes.” Nature Reviews Molecular Cell Biology 19(6):382–98. doi: 10.1038/s41580-018-0004-3.

Sahabandu, N., D. Kong, V. Magidson, R. Nanjundappa, C. Sullenberger, M. R. Mahjoub, and J. Loncarek. 2019. “Expansion Microscopy for the Analysis of Centrioles and Cilia.” Journal of Microscopy 276(3):145–59. doi: 10.1111/jmi.12841.

Stendahl, John C., Dixon B. Kaufman, and Samuel I. Stupp. 2009. “Extracellular Matrix in Pancreatic Islets: Relevance to Scaffold Design and Transplantation.” Cell Transplantation 18(1):1–12. doi: 10.3727/096368909788237195.

Sviben, Sanja, Alexander J. Polino, Isabella L. Melena, and Jing W. Hughes. 2024. “Immuno-Scanning Electron Microscopy of Islet Primary Cilia.” Journal of Cell Science 137(20):jcs262038. doi: 10.1242/jcs.262038.

Uzbekov, Rustem, Anastasiia Garanina, and Christophe Bressac. 2018. “Centrioles without Microtubules: A New Morphological Type of Centriole.” Biology Open 7(8):bio036012. doi: 10.1242/bio.036012.

Viswanadha, Rasagnya, Winfield S. Sale, and Mary E. Porter. 2017. “Ciliary Motility: Regulation of Axonemal Dynein Motors.” Cold Spring Harbor Perspectives in Biology 9(8):a018325. doi: 10.1101/cshperspect.a018325.

Yoon, Joshua, Colin J. Comerci, Lucien E. Weiss, Ljiljana Milenkovic, Tim Stearns, and W. E. Moerner. 2019. “Revealing Nanoscale Morphology of the Primary Cilium Using Super-Resolution Fluorescence Microscopy.” Biophysical Journal 116(2):319–29. doi: 10.1016/j.bpj.2018.11.3136.

Zariwala, Maimoona A., Margaret W. Leigh, Franck Ceppa, Marcus P. Kennedy, Peadar G. Noone, Johnny L. Carson, Milan J. Hazucha, Adriana Lori, Judit Horvath, Heike Olbrich, Niki T. Loges, Anne-Marie Bridoux, Gaëlle Pennarun, Bénédicte Duriez, Estelle Escudier, Hannah M. Mitchison, Rahul Chodhari, Eddie M. K. Chung, Lucy C. Morgan, Robbert U. de Iongh, Jonathan Rutland, Ugo Pradal, Heymut Omran, Serge Amselem, and Michael R. Knowles. 2006. “Mutations of DNAI1 in Primary Ciliary Dyskinesia.” American Journal of Respiratory and Critical Care Medicine 174(8):858–66. doi: 10.1164/rccm.200603-370OC.

Ziętkiewicz, Ewa, Barbara Nitka, Katarzyna Voelkel, Urszula Skrzypczak, Zuzanna Bukowy, Ewa Rutkiewicz, Kinga Humińska, Hanna Przystałowska, Andrzej Pogorzelski, and Michał Witt. 2010. “Population Specificity of the DNAI1 Gene Mutation Spectrum in Primary Ciliary Dyskinesia (PCD).” Respiratory Research 11(1):174. doi: 10.1186/1465-9921-11-174.